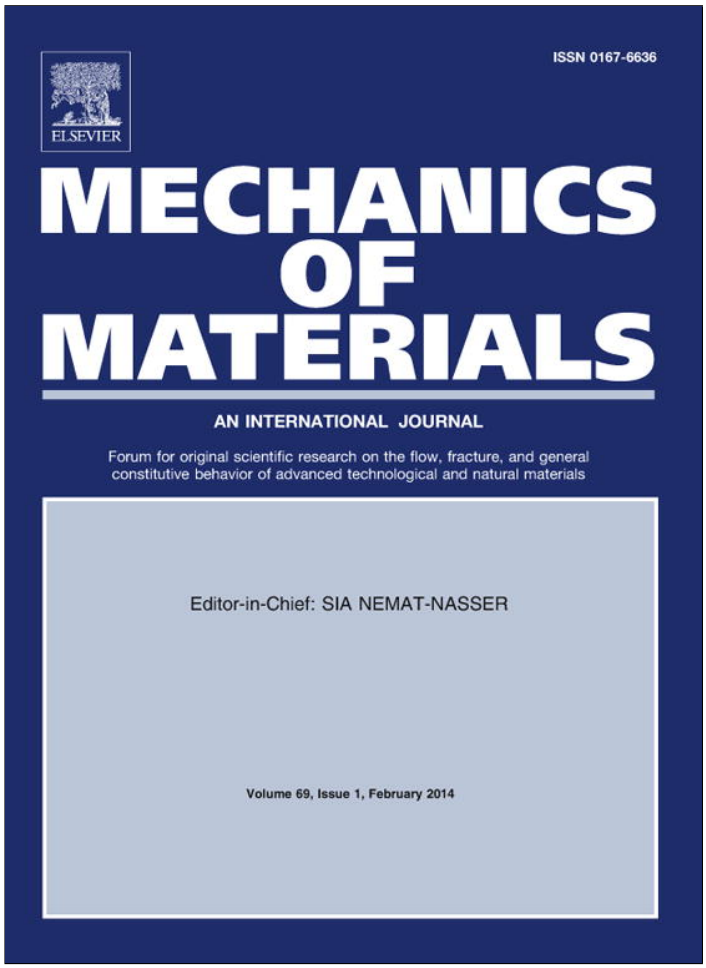

Mechanics of Materials 69 (2014) 251–261

Contents lists available at ScienceDirect

Mechanics of Materials

journal homepage: www.elsevier.com/locate/mechmat

Composites with fractal microstructure: The effect of long range correlations on elastic–plastic and damping behavior

R.C. Picu [a,*], Z. Li [a], M.A. Soare [b], S. Sorohan [c], D.M. Constantinescu [c], E. Nutu [c]

[a] Department of Mechanical, Aerospace and Nuclear Engineering, Rensselaer Polytechnic Institute, Troy, NY 12180, United States
[b] General Electric Global Research, Niskayuna, NY 12309, United States
[c] Department of Strength of Materials, University POLITEHNICA of Bucharest, Bucharest, Romania

ARTICLE INFO

Article history:
Received 14 June 2013
Received in revised form 22 October 2013
Available online 22 November 2013

Keywords:
Fractals
Damping
Plastic deformation
Toughening

ABSTRACT

The effect of correlations of the spatial distribution of inclusions in a two-phase composite is studied numerically in this work. Microstructures with fractal distribution of inclusions, characterized by long-range power law correlations, are compared with random inclusion distributions of same volume fraction. The elastic–plastic response of composites with stiff elastic inclusions and elastic–plastic matrix is studied, and it is concluded that fractal microstructures always lead to stiffer composites, with higher strain hardening rates, compared with the equivalent composites with randomly distributed inclusions. Composites with filler distributions characterized by shorter range, exponential correlations exhibit behavior intermediate between that of random and power law-correlated microstructures. Larger variability from replica to replica is observed in the fractal case. The pressure in inclusions is larger in the case of fractal microstructures, indicating that these are expected to be advantageous in applications such as toughening of thermoset polymers which takes place via the cavitation mechanism. The effect of the spatial distribution of inclusions on the effective damping of the composite is also investigated. The matrix is considered elastic and non-dissipative, while inclusions dissipate energy. The composite with fractal microstructure provides more damping than the random microstructure of same filler volume fraction, and the effect increases with increasing fractal dimension. When damping is introduced only in the interfaces between matrix and inclusions, the spatial distribution of fillers becomes inconsequential for the overall composite behavior. These results are relevant for the design of composites with hierarchical multiscale structure.

1. Introduction

Composite materials are broadly used in engineering for their properties emerging from the interaction of the constituent phases. In most man-made composites the structure is either random or periodic. Particulate composites, made by mixing inclusions of nominally monodisperse dimensions in a matrix, have a random microstructure. In many other situations, manufacturing processes lead to periodic microstructures, as for example in woven fiber composites. Therefore, the distribution of inclusions in the matrix is dictated primarily by technological reasons and not by considerations related to the optimization of system level properties of the material.

Exceptions to this rule are structures designed by an optimization scheme aimed at achieving an optimum of an objective function representing one or multiple macroscopic properties. Such structures can be produced only by specialized techniques lacking high throughput, such as additive manufacturing (e.g. Vaezi et al., 2012).

Biological materials, on the other hand, have complex microstructures which are optimized to perform a certain function while using the minimum volume of material.

* Corresponding author. Tel.: +1 518 276 2195.
E-mail address: picuc@rpi.edu (R.C. Picu).

0167-6636/$ - see front matter © 2013 Elsevier Ltd. All rights reserved.
http://dx.doi.org/10.1016/j.mechmat.2013.11.002

Examples are the trabecular bone (Parkinson and Fazzalari, 2000) and various types of marine shells (Meyers et al., 2006). Mass is distributed in the trabecular bone only in regions carrying large stresses, while in shells structural elements are distributed in layers such to maximize strength and toughness. Most of these materials are hierarchical and some are self-similar across a range of scales. These structures have some degree of stochasticity and are either only approximately periodic (e.g. the structure of abalone shells) or lack translational symmetry all together (e.g. the trabecular bone).

It is useful to ask why nature designs structures with self-similar multiscale structure. In the context of engineered materials, one may alternatively ask how inclusions should be distributed in a composite to maximize macroscopic properties, while preserving some level of stochasticity, which is mandated by the technological need to produce such materials at reasonable cost and in large volumes. This is the objective of the current work.

Specifically, while acknowledging that the volume fraction of inclusions is the major factor controlling the properties of the composite, we inquire what benefits may be obtained if the reinforcing phase is distributed in a spatially correlated way. To address this question, we compare random and spatially correlated distributions of inclusions. The limit case of a spatially correlated microstructure is a fractal, in which correlations are described by a power law and the exponent of the correlation function depends on the fractal dimension (Falconer, 2003). Fractal microstructures lack translational symmetry, but have scaling symmetry, i.e. remain self-similar upon a scaling operation (Mandelbrot, 1983; Falconer, 2003). The properties of interest are the elastic–plastic response and the damping behavior of the composite. Damping is of interest in applications in which the material is subjected to intense vibrations (e.g. composites used for helicopter blades) and inclusions are added to enhance energy dissipation, while providing stiffness and strength. Damping may take place in the volume of inclusions or/and at the interface with the matrix. Another problem of interest is toughening of brittle polymers (thermosets) by the addition of rubbery inclusions. Toughening is triggered in such situations by cavitation within inclusions. This process is driven by the hydrostatic stress component. Inclusions are usually distributed randomly in the polymer volume and it is interesting to inquire if a different stochastic distribution could lead to larger toughening at prescribed filler volume fraction.

The effect of the distribution of inclusions on the elastic moduli of composites has been studied for a long time. Reviews on the homogenization of random composites are presented in Nemat-Nasser and Hori (1999), Torquato (2002) and Dvorak (2013). Remarkable results have been obtained regarding the bounds on the elastic moduli of such composites. These expressions are generally given in terms of the volume fraction of the constituents. The closest bounds for the bulk modulus which take into account only the volume fraction have been derived by Hashin and Shtrikman (HS) (Hashin and Shtrikman, 1962). A family of higher order bounds, which take into account statistical measures of the microstructure geometry, have been proposed more recently with the purpose of reducing the separation between the upper and lower bounds (e.g. Beran and Molyeux, 1966; Silnutzer, 1972; Milton, 1981; Milton, 1982; Phan-Tien and Milton, 1982; Quinatanilla and Torquato, 1995). The n-point bounds are written in terms of n-point microstructural correlation functions which define the probability that n points with specified relative positions are all located in a certain phase of the composite. Any statistical correlation of the microstructure can be accounted for by using these methods. A review of the higher order bounds and the geometric parameters required for their evaluation is provided in Torquato (2002).

Fractal structures have been studied in connection with various physical processes such as transport (Dzhaparidze and van Zanten, 2003), diffusion limited aggregation (Witten and Sander, 1983), and dislocation patterning during deformation of metals (Zaiser and Hahner, 1999; Bako and Hoffelner, 2007), microscale plasticity (Chen et al., 2010; Ostoja-Starzewski, 2012). Fractal concepts were also used in percolation theory (Bergman and Kantor, 1984), quantum mechanics (Argyris et al., 2000), fracture mechanics (Bazant, 1997), etc. However, despite its practical importance, very few attempts have been made to study the deformation of such structures or that of composites containing fractal inclusions.

The elastic moduli of deterministic fractal structures have been predicted using standard finite element models and renormalization group concepts to extrapolate to the range of scales not accessible by direct simulation (Oshmyan et al., 2001). Dyskin applied the differential self-consistent method (initiated in Salganik (1973)) for media containing self-similar distributions of spherical/ellipsoidal pores or cracks (Dyskin, 2005). The author proposes to model such materials by a sequence of continua with effective elastic properties. This does not take into account the interaction of inclusions. Other approaches consider the reformulation of the governing equations to account for the fractal nature of the inclusion domains. Tarasov studied porous materials having pores with a broad range of sizes and in which the mass of the material within a volume of dimension R scales as $m(R) \prec R^Q$, with Q non-integer (Tarasov, 2005a,b). The author replaces the fractal body with an equivalent continuum governed by a "fractal metric". The balance equations for mass, linear and angular momentum for the equivalent continuum are reformulated in terms of this metric. This method was further developed recently in Ostoja-Starzewski (2007, 2009) to represent the mechanics of heterogeneous bodies with fractal microstructure.

Carpinteri et al. studied the deformation of a bar in which the strain is localized in a subset of cross-sections forming a Cantor set (Carpinteri et al., 2004). These authors use fractional operators to rewrite the balance equations, although in one dimension this is not immediately necessary. The deformation of a two-dimensional composite with Cantor-like inclusion distribution was studied in Soare and Picu (2007). A numerical method using enriched shape functions that account for the finer scale geometry was developed in this work and was applied to structures with an arbitrary number of scales.

In Picu and Soare (2009) fractional calculus based on local fractional operators introduced by Kolwankar and

Gangal (1996) and Kolwankar (1998) were used to formulate the balance equations on the fractal support. The formulation was applied to modeling the deformation of two-dimensional composites containing a fractal distribution of inclusions in a matrix. The method is readily extendable to three-dimensional composites.

In the stochastic case, in addition to Monte Carlo (MC) methods (Papadrakakis and Papadopoulos, 1996), various systematic ways of approaching numerically partial differential equations defined on single-scale stochastic domains were proposed in the literature. Methods based on probabilistic finite elements (second order perturbation PFEM) (Liu et al., 1986, 1987), or the spectral approach for stochastic finite elements (SSFEM) (Ghanem and Spanos, 1991) are relevant examples. These methods were applied to various problems in solid and fluid mechanics such as for example to study transport through porous media (Ghanem and Dham, 1998) and elastic deformation (Matthies et al., 1997). The elastic deformation of composites with fractal microstructure was represented using the stochastic finite element method in Soare and Picu (2008a) based on an approximation of the spectral decomposition of the representation of the fractal microstructure presented in Soare and Picu (2008b).

In most problems involving fractal microstructures studied to date, the mechanical behavior of interest was either the dynamic or the quasistatic elastic response. In the present work we use ensemble averaging of realizations modeled using finite elements and investigate a broader range of mechanical properties, as mentioned above. This allows investigating not only the global composite behavior, but also the local stress distribution, which is relevant in damage nucleation and evolution.

The article begins with an overview of the models and methods used (Section 2), and continues with results pertaining to the elastic–plastic deformation (Section 3.1), internal stresses in structures subjected to quasistatic deformation (Section 3.2), and the investigation of the effect of the distribution of inclusions on the damping behavior of the composite (Section 3.3). Conclusions are presented in closure.

2. Models and methods

Two phase two-dimensional composites are considered. The matrix fills the Euclidean space of the problem domain. In each realization, inclusions form a fractal which is a generalization of the classical Cantor set to probabilistic structures embedded in 2D (Soare and Picu, 2008a). The microstructure is constructed hierarchically by iteratively applying a set of transformation rules. The first generation (approximation of the fractal set with an infinite number of scales) is obtained by starting with an Euclidean domain, dividing it in M equal cells and selecting randomly P of them which are to be filled by inclusions. The characteristic length of these inclusions is ε_1. The number of possible configurations at the first generation is $M!/(P!(M-P)!)$. The next generations are obtained by dividing again each of the fractal cells in M equal parts from which $M-P$ are transformed into "matrix" cells. Thus, the approximation of the domain A at a certain scale n, A_n, is seen as a reunion of M^n cells of characteristic dimension ε_n, of which P^n are occupied by the inclusion (fractal) material. The remaining $M^n - P^n$ cells are occupied by the matrix. The number of possible configurations at iteration, n, is $[M!/(P!(cM-P)!)]^{p^{n-1}+\cdots+p+1}$. The volume fraction of inclusions is given by $f=(P/M)^n$, while the fractal dimension of the set is $D=2\log(P)/\log(M)$. The natural numbers M ($M \geqslant 2$) and P ($1 \leqslant P < M$) are kept as parameters in this analysis. Fig. 1(a) shows a realization of a composite with $M=9$, $P=6$ and $n=5$, which has volume fraction $f=13.1\%$ and fractal dimension $D=1.63$. Note that the fractal dimension is smaller than 2, the dimension of the embedding space.

It is important to observe that the set of inclusions represents a fractal object only in the range of scales defined by the smallest representative length, ε_n, and the largest length scale of the problem. If the upper bound (the dimension of the structure in Fig. 1(a)) is taken to be L, one computes $\varepsilon_n = L/M^{n/2}$, or $\varepsilon_5 = L/243$ for Fig. 1(a). For any set with given ε_n, the object is non-fractal and with dimension equal to that of the embedding space at all length scales smaller than ε_n. The composite is not defined on scales larger than L in the present case, since the boundary conditions are defined at this scale. The fractal object does not have translation symmetry, rather it has scaling symmetry. For example, one may fill the embedding space with replicas of the fractal set bounded by L and ε_n, but the resulting structure will have translation symmetry on scales larger than L, and scaling symmetry between L and ε_n.

An important property related to the present discussion is that the fractal structure has long range, power law correlations. Consider the characteristic function defined on the fractal support, taking values of 1 in inclusions and 0 elsewhere: $h(x_1,x_2)=1$ if $(x_1,x_2)\in A_n$, and $h(x_1,x_2)=0$ if $(x_1,x_2)\in A-A_n$. This function is probed with resolution ε_n. On scales larger than ε_n one has $ACF(r)=h(x_1+r,x_2)\,h(x_1,x_2)_{(x_1,x_2)} \sim r^{-4+2D}$, as $r\to\infty$ (Falconer, 2003; Gneiting and Schlather, 2004), where $\langle x\rangle_{(x_1,x_2)}$ indicates ensemble averaging over all points defined by the coordinate pair (x_1, x_2). Due to its stochastic isotropy, the fractal object has $ACF(r)=h(x_1+\alpha_1,x_2+\alpha_2)h(x_1,x_2)_{(x_1,x_2)} \sim r^{-4+2D}$, with $r^2=\alpha_1^2+\alpha_2^2$.

The behavior of these structures is compared with that of composites with random distribution of inclusions of same volume fraction and having the same characteristic length ε_n, which, in this case, represents the size of the randomly distributed inclusions. Fig. 1(b) shows a realization of a random structure having the same f and ε_n as the structure in Fig. 1(a). The correlation of the characteristic function h of the random microstructure is a Delta function of variable r when probed with resolution ε_n. Comparing the mechanical behavior of composites similar to those in Fig. 1(a) and (b) provides insight into the role of spatial correlations of the position of inclusions in defining the composite mechanics.

In order to put this discussion in perspective, we have also considered composites in which the position of inclusions is exponentially correlated. An example is shown in Fig. 1(c). This structure has the same parameters f and ε_n with those in Fig. 1(a) and (b), but has

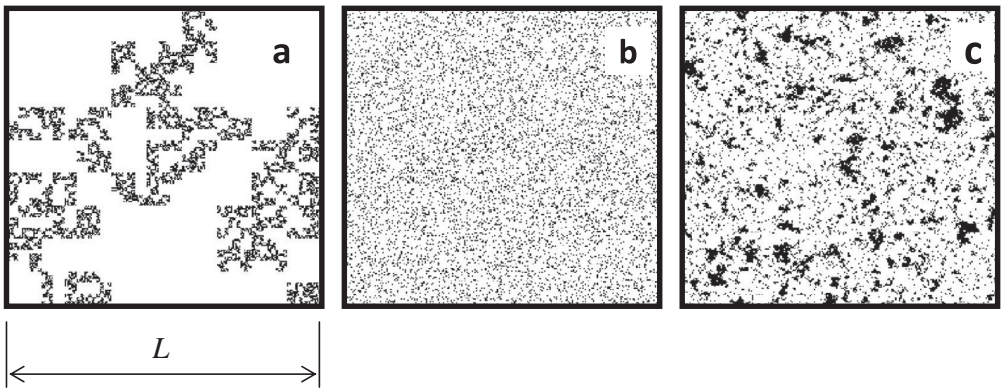

Fig. 1. The three types of composite microstructures studied in this work. The matrix is shown in white and inclusions in black. (a) Fractal distribution of inclusions with $M = 9$, $P = 6$ and $n = 5$. The smallest length scale, or the dimension of an isolated inclusion is $\varepsilon_n = \varepsilon_5 = L/243$. The volume fraction of inclusions is $f = 0.131$ and the fractal dimension is $D = 1.63$. (b) Random distribution of inclusions of same f and ε_n. (c) Microstructure characterized by an exponential correlation function of inclusion positions and having the same f and ε_n as the fractal structure in (a).

$ACF(r) = h(x_1 + \alpha_1, x_2 + \alpha_2)h(x_1, x_2)_{(x_1,x_2)} \sim \exp(-r/r_0)$ for all pairs α_1 and α_2 having the property $r^2 = \alpha_1^2 + \alpha_2^2$, and with r_0 a constant. The specific situations in which such structures are used and the parameters involved (e.g. r_0), are discussed in Section 3.1.

It is of interest to outline the method used to generate the exponentially correlated samples. To this end, domain A is partitioned on scale ε_n. On the resulting square lattice, the characteristic function takes random binary values, 0 and 1. An Ising model is then used to evolve the system. The Ising model has been extensively studied in statistical physics and was used to model phase transitions in many systems, e.g. see Baxter (1982). In the present context, each cell is assigned a spin (either $s = +1$ or $s = -1$) depending on the local value of the characteristic function. The spins interact such that the total energy of the system in absence of an external field is $E = -\sum_{\{i,j\}} J s_i s_j$, where the summation is performed over all interacting cells/spins $\{i, j\}$. Parameter J can be selected to depend on the relative position of the two cells i and j. The system is evolved using a Monte Carlo procedure which is controlled by a temperature-like parameter, $\beta = 1/k_B T$. When the dimensionality is larger than one, the mean field solution of this model predicts a phase transition once the temperature decreases below a critical value, or $\beta > \beta_c$. For $\beta < \beta_c$, spins are random and the total magnetization, $\langle s \rangle$, vanishes. Below the critical value, the system acquires a net magnetization. In the language of the present application, when $\beta < \beta_c$, function h is either 0 or 1 with equal probability, and $f = 0.5$. For $\beta > \beta_c$, one of the two phases dominates and h can be adjusted such to obtain the volume fraction, f, in the desired range of values. To this end, β is selected in the close vicinity of the critical point. Numerical Ising models have provided a richer physics which could not be captured by the mean field approach. The system exhibits residual magnetization even above the critical temperature due to spin clustering and the phase transition takes place gradually.

The interesting property of the Ising model is that it provides exponential spatial correlations, or clustering, of the spins and the correlation of the characteristic function h is exponentially decaying. The range can be adjusted, to some extent, by controlling the constant J in the energy function and its dependence on the distance between the interacting spins, s_i and s_j. In this work, interactions are considered up to the second nearest neighbors of the square lattice. The interaction strength is $J = 2.5$ for both first and second nearest neighbors. The temperature parameter β was kept in the close vicinity of the critical point provided by the mean field solution, $\beta_c = 2/(zJ)$, where z is the number of interacting neighbors of each site.

Fig. 2 shows the correlation function obtained using this procedure and corresponding to Fig. 1(c), along with the power correlation function corresponding to the fractal microstructure of Fig. 1(a). The random distribution of Fig. 1(b) leads to a Delta function centered at zero and is not shown in Fig. 2. The corresponding best fits to the two curves in Fig. 2, exponential and power law, are also shown. Note that the characteristic length of the exponential function, r_0, is selected such that it provides a reasonable approximation for the power law correlation

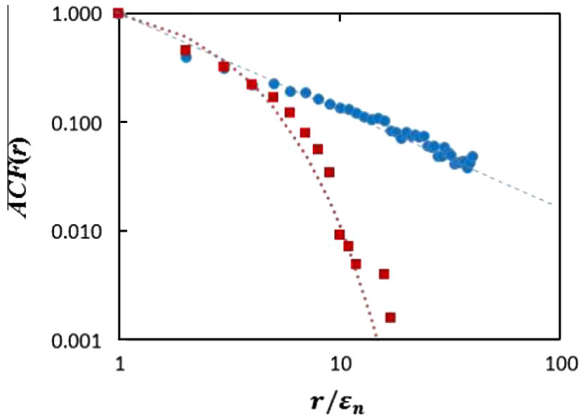

Fig. 2. Normalized $ACF(r)$ functions for a fractal microstructure with $M = 9$, $P = 5$ and $n = 4$ (blue circles) having $D = 1.46$ and $f = 0.131$, and for a clustered microstructure similar to that in Fig. 1(c) and with $f = 0.131$ (filled red squares). The functions are normalized by the variance $ACF(0)$. The dotted red line represents an exponential fit to the ACF of the clustered microstructure. The slope of the blue dashed line is -0.95. (For interpretation of the references to color in this figure legend, the reader is referred to the web version of this article.)

in the vicinity of the origin. The exponential correlation has an early cut-off at $r > r_0 \sim 4\varepsilon_n$, while the decay of the correlation function of the fractal is much slower and the correlation function is much longer ranged.

These microstructures are discretized and their mechanical response is determined with a finite element model. We have used the commercial finite element package Ansys for all simulations. The two-dimensional simulation domain for each representation is a square of length L, which is meshed uniformly with 4-node plane stress elements. At a given M value, the same level of refinement is maintained for all scales, n. For example, all structures with $M = 9$ and $n = 2$–5 are meshed with 972^2 elements, i.e. with elements of size $\varepsilon_n/4$, where ε_n corresponds to $n = 5$. We have tested in representative cases that further mesh refinement does not lead to significantly different system-scale results. Furthermore, we checked that at this level of mesh refinement the use of 8-node elements does not lead to different results.

Model size effects are usually a concern when analyzing structures with spatial correlations. In the case of randomly distributed inclusions, the model size should be at least an order of magnitude larger than the characteristic size of inclusions in order to insure that the results are model size-effect free (Dvorak, 2013). This insures scale decoupling between the characteristic length scale of the microstructure and the scale of observation/homogenization. A similar rule applies in presence of correlations. For example, in the case of the exponentially correlated microstructures of Fig. 1(c), L should be an order of magnitude larger than r_0 (here $r_0 \sim 4\varepsilon_n$ and $L = 243\varepsilon_n$). The case of the fractal microstructures is different as the geometry is scale-free and hence correlation decay is power law. The behavior of these structures is intrinsically dependent on the two scale (upper, L, and lower, ε_n) at which the hierarchy is truncated. This "size effect" is an intrinsic property of the fractal microstructures which, we suggest, can be used to advantage in material design.

In models used to determine the elastic–plastic response, inclusions are linear elastic with Young's modulus and Poisson ratio E_2 and ν_2, while the matrix is represented with a bi-linear model with slopes E_1 and $0.1E_1$ in the elastic and plastic regimes, respectively. In all simulations $E_2 = 6E_1$, $\nu_1 = \nu_2 = 0.3$ and kinematic hardening is used for the plastic range. The yield strain of the matrix material is 0.01. In models used to study the damping behavior of the composite, the two materials are linear elastic and isotropic with $E_2 = 6E_1$ and $\nu_1 = \nu_2 = 0.3$. Parameters characterizing damping are discussed in Section 3.4. In all cases discussed below, stress is normalized by E_1 and displacements by L.

3. Results and discussion

Structures with fractal and random microstructures are studied with respect to their elastic–plastic and damping behavior. The central question posed refers to the role of the distribution of heterogeneity in defining the overall response of the composite.

3.1. Elastic–plastic behavior

Structures similar to those shown in Fig. 1 are considered for this study. The matrix fills the square problem domain and embeds inclusions of dimension ε_n. Stress–strain curves are computed for 100 realizations, each being loaded uniaxially in displacement control up to a global strain of 2%. The boundaries in the direction perpendicular to the loading direction are traction free. The stress–strain curves and all subsequent plots represent the ensemble average stress. The standard deviation is below 1% for the random case and approximately 5% for the fractal case (which is about the size of the symbols used in Fig. 3).

Fig. 3 shows results for two fractal microstructures with $M = 9$, $P = 5$ and $n = 2$ and 3, respectively (filled symbols), and random microstructures of the same volume fraction (open symbols). The volume fractions are $f = 0.308$ and 0.171 for $n = 2$ and 3, respectively. It is seen that all curves are bilinear, and that at the same volume fraction the curve corresponding to the fractal case is above that for the random microstructures. However, the probability that two specific realizations with fractal and random microstructures lead to stress–strain curves which are in the reverse order is not zero. As n increases, f decreases and hence the curves asymptote to the stress–strain curve of the matrix (shown by the continuous line in Fig. 3). Furthermore, as n increases, the distinction between the curves for fractal and random cases decreases since the volume fraction f decreases.

The effective elastic modulus of the composite, E_e, and the strain hardening rate defined by the slope E_p, can be evaluated from the stress-strain curves as suggested in Fig. 3. These two parameters fully define the uniaxial response of the composite, therefore we focus attention on their dependence on the fractal dimension, D, and the volume fraction, f. Specifically, the fractal dimension controls the exponent of the autocorrelation power function and hence comparing fractal structures with same f and various D, one may infer the effect of the spatial correlation of the distribution of heterogeneity on the overall composite response.

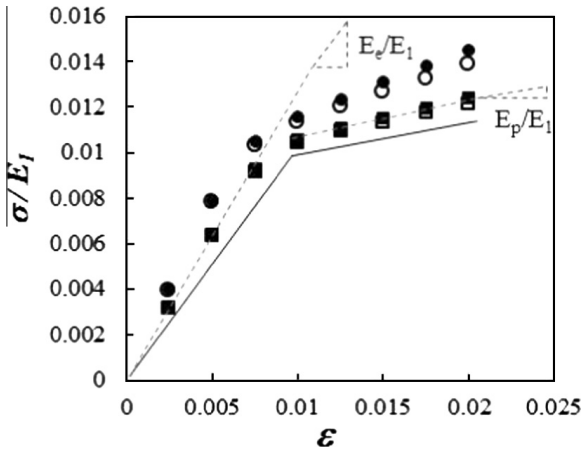

Fig. 3. Stress–strain curves for composites with fractal microstructure (filled symbols) and random microstructures of same volume fraction (open symbols), with $M = 9$, $P = 5$, $n = 2$ (circles) and $M = 9$, $P = 5$, $n = 3$ (squares). The continuous line represents the mechanical behavior of the matrix material. The dashed lines define slopes E_e and E_p.

Fig. 4(a) shows the variation of the elastic modulus, E_e/E_1, with the volume fraction, f, for random structures (open symbols), and various fractal structures. Data are shown for $M = 9$, $P = 5$, and $n = 2$–5 (blue circles), which all have $D = 1.46$, for $M = 4$, $P = 3$, $n = 7$ and 8 (green squares), which have $D = 1.58$, and for $M = 81$, $P = 42$, $n = 2$ and 3 (red triangles), which have $D = 1.7$. These structures have different filler volume fractions. Obtaining fractal geometries with the same f and various D values is not possible. The thick continuous orange lines represent the Hashin–Shtrikman bounds for the two-dimensional case (Hashin and Shtrikman, 1962; Hashin, 1965).

The data points for the random microstructures align on a curve described by Eq. (1) and shown by the continuous thin line in Fig. 4(a).

$$E_e/E_1 = 1.73f^2 + 1.27f + 1 \tag{1}$$

The four data points corresponding to fractal structures with $M = 9$, $P = 5$, $D = 1.46$, are well represented by a similar curve, which is shown by the dashed line in Fig. 4(a). It is possible to approximate all data with the expression:

$$E_e/E_1 = 1.73gf^2 + 1.27gf + 1 \tag{2}$$

with $g = 0.2(3D + 1)$, which holds for $D > 1.3$ This indicates that the stiffness increases with D, which is a consequence of the stronger interaction of inclusions in the fractal structures.

The influence of filler packing on the elastic moduli has been discussed before. The properties of fiber composites loaded perpendicular to the preferential direction of fibers have been determined for a variety of periodic arrangements (e.g. Brockenbrough et al., 1991; Nakamura and Suresh, 1993). For random microstructures one can make use of the n-point bounds derived in the homogenization literature (for a review see Torquato (2002)) to investigate the expected variation of the elastic constants in presence of long range correlations. The three point bounds for the bulk (K_l, K_u) and shear (G_l, G_u moduli in two dimensions are given by Milton (1982) and Torquato (2002):

$$K_u = \langle K\rangle - \frac{f(1-f)(K_2-K_1)^2}{\langle\tilde{K}\rangle + \langle G\rangle_\xi};$$
$$K_l = \langle K\rangle - \frac{f(1-f)(K_2-K_1)^2}{\langle\tilde{K}\rangle + (\langle G^{-1}\rangle_\xi)^{-1}} \tag{3a}$$

$$G_u = \langle G\rangle - \frac{f(1-f)(G_2-G_1)^2}{\langle\tilde{G}\rangle + \Theta};$$
$$G_l = \langle G\rangle - \frac{f(1-f)(G_2-G_1)^2}{\langle\tilde{G}\rangle + \Psi} \tag{3b}$$

where $\langle z\rangle = (1-f)z_1 + fz_2$, $\langle\tilde{z}\rangle = (1-f)z_2 + fz_1$, and $\langle z\rangle_\xi = (1-\xi_2)z_1 + \xi_2 z_2$ for any quantity, z, and defining phase 2 as the stiffer inclusions and phase 1 being the matrix. Parameters Θ and Ψ in Eq. (3b) are given by:

$$\Theta = \frac{2\langle K\rangle_\xi\langle G\rangle^2 + \langle K\rangle^2\langle G\rangle_\eta}{\langle K+2G\rangle^2} \tag{4a}$$

$$\Psi^{-1} = 2\langle K^{-1}\rangle_\xi + \langle G^{-1}\rangle_\eta \tag{4b}$$

The bounds for Young's modulus, E, are computed using Eq. (3) and the 2D relationship between the three types of moduli, $4/E = 1/G + 1/K$.

ξ and η, are 3-point parameters characterizing the distribution of inclusions (phase 2) in the matrix. These are given for the two-dimensional case by Milton (1982) and Torquato (2002):

$$\xi_2 = \frac{4}{\pi f(1-f)}\int_0^\infty \frac{dr}{r}\int_0^\infty \frac{ds}{s}\int_0^\pi d\theta'\cos(2\theta') \times [S_3(r,s,t) - S_2(r)S_2(s)/f] \tag{5a}$$

$$\eta_2 = \frac{16}{\pi f(1-f)}\int_0^\infty \frac{dr}{r}\int_0^\infty \frac{ds}{s}\int_0^\pi d\theta'\cos(4\theta') \times [S_3(r,s,t) - S_2(r)S_2(s)/f] \tag{5b}$$

where $S_2(z)$ is the 2-point correlation function representing the probability that the ends of a segment of length z are

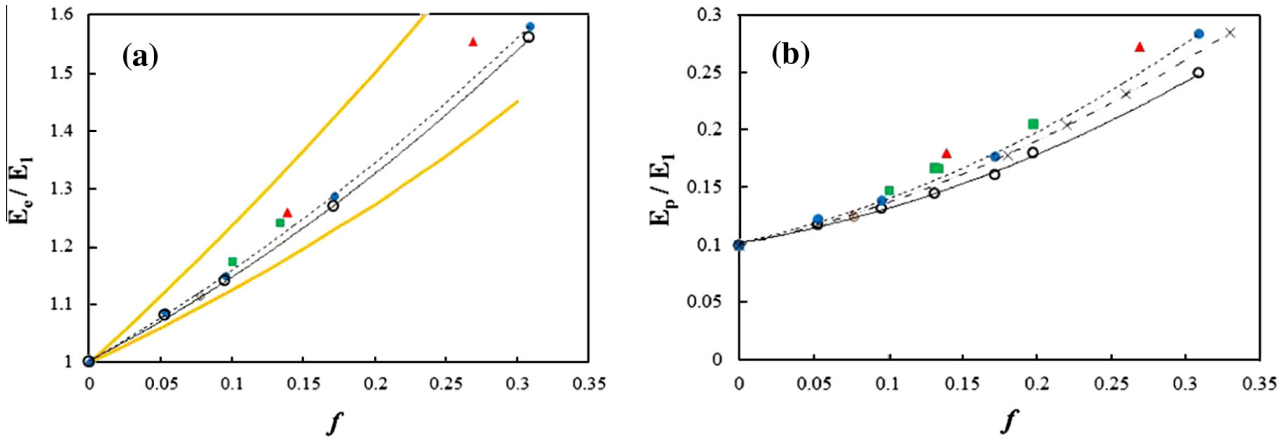

Fig. 4. Variation of (a) the elastic modulus (E_e/E_1), and (b) strain hardening rate (E_p/E_1) with the volume fraction, for microstructures with randomly distributed inclusions (open symbols and continuous thin line), and for various fractal microstructures having $M = 9$, $P = 5$, and $n = 2$–5 (blue circles), $M = 4$, $P = 3$, $n = 7$ and 8, $M = 9$, $P = 6$, $n = 4$ and 5 (green squares), $M = 81$, $P = 42$, $n = 2$ and 3 (red triangles). Data for microstructures with exponential correlation function (Fig. 1(c)) are shown in (b) with crosses and dashed-dot line. The thick orange continuous lines in (a) represent the 2D Hashin–Shtrikman bounds. The thin continuous line and the dashed line in both (a) and (b) represent the best fit to the random structures data and to the fractal structures with $M = 9$, $P = 5$, respectively. (For interpretation of the references to color in this figure legend, the reader is referred to the web version of this article.)

both in phase 2, and $S_3(z_1, z_2, z_3)$ is the 3-point correlation function representing the probability that all corners of a triangle of edge lengths z_1, z_2, z_3 are in phase 2. Length t is computed in terms of r, s and θ' as $t^2 = r^2 + s^2 - 2rs\cos(\theta')$.

The 2-point correlation function is evaluated numerically from the microstructure. For all microstructures studied S_2 has the limit values $S_2(0) = f$ and $S_2(\infty) = f^2$. For the random microstructure $S_2(r) = f^2$ for all $r > \varepsilon_n$. The fractal microstructures lead to S_2 functions with power law decay on scales $r > \varepsilon_n$. The 3-point correlation function S_3 is estimated using the approximation in terms of 2-point correlation functions proposed in Banissadi et al. (2012):

$$S_3(r,s,t) \approx \frac{t}{r+s+t}\frac{S_2(r)S_2(s)}{f} + \frac{s}{r+s+t}\frac{S_2(r)S_2(t)}{f} + \frac{r}{r+s+t}\frac{S_2(t)S_2(s)}{f} \quad (6)$$

which is reported to provide estimates with a maximum error of 20%. The value of ξ_2 computed using Eq. (5a) for the random microstructure with $f = 0.0953$ is $\xi_2 = 0.33$. This is larger than the value predicted with the formula $\xi_2 = 0.08079(1-f) + 0.91921f$ ($\xi_2 = 0.1607$) proposed in the literature for symmetric-cell materials of checkerboard type (Torquato, 2002). For the same random microstructure we obtain $\eta_2 = 0.126$ using Eq. (5b). The corresponding parameters for the fractal microstructure with $M = 9$, $P = 5$, $n = 4$ ($D = 1.465$, $f = 0.0953$) are $\xi_2 = 0.373$ and $\eta_2 = 0.212$.

The HS bounds are compared with the 3-point bounds evaluated using Eqs. (3) and (4) in Fig. 5. The range defined by the higher order bounds is much narrower than that defined by the HS bounds, as expected. The observation relevant for the present discussion is that both 3-point bounds shift up as the range of spatial correlations increases, which is in agreement with the generic trend reported in this article for all effective properties discussed. In fact, considering that as the correlation range increases, parameters ξ_2 and η_2 increase, this trend can be inferred directly from Eq. (3) without the need to perform a numerical study.

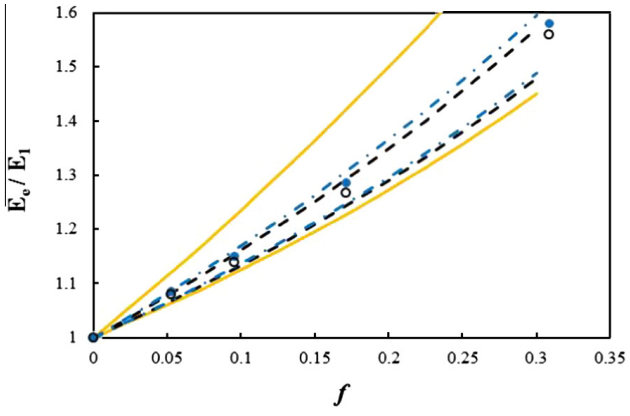

Fig. 5. Hashin–Shtirkman bounds (continuous orange lines) and 3-point bounds for the random (dashed black curves) and fractal (dash-dot blue curves) microstructures. The symbols represent the effective moduli of fractal microstructures with $M = 9$, $P = 5$, and $n = 2$–5 (blue circles), and of random microstructures of same volume fraction f, from Fig. 4a. (For interpretation of the references to color in this figure legend, the reader is referred to the web version of this article.)

Fig. 4(b) shows the normalized strain hardening rate versus the filler volume fraction for composites with random microstructures, composites with microstructures having exponential correlations, and fractal microstructures with parameters similar to those discussed in relation to Fig. 4(a). The strain hardening rate is independent of strain since the composite has a bilinear stress–strain curve. It is seen that all microstructures with spatial correlations of the distribution of inclusions have larger strain hardening rates than the random microstructures. The longer ranged the correlation, the larger is the value of E_p. The fractal dimensions of the fractal microstructures considered is $D = 1.43$, 1.58, 1.63 and 1.7, for the structures with ($M = 9$, $P = 5$), ($M = 4$, $P = 3$), ($M = 9$, $P = 6$) and ($M = 81$, $P = 42$), respectively. It is apparent that as D increases, the data move to higher values of E_p.

An interesting comparison can be made between the fractal system with $M = 9$, $P = 5$ and the system with exponential correlations. The correlation functions for these two types of structures are shown in Fig. 2. The exponential correlation is selected such to approximately match the power law correlation of the fractal structures at small values of r/ε_n. The data in Fig. 4(b) indicate that the strain hardening rate of the fractal microstructure is always larger than that of the microstructure with exponential correlations. This indicates the effect of the range of spatial correlations: as this parameter increases, the effective modulus, E_e/E_1, and the strain hardening rate, E_p/E_1, increase. This is attributed to the enhanced interaction of inclusions in the microstructures with non-random distributions of inclusions.

The effect of filler packing on strain hardening rates was observed before for periodic structures in 2D plane strain models (Brockenbrough et al., 1991; Nakamura and Suresh, 1993; Suresh and Brockenbrough, 1993). For example, it was observed that the strain hardening rate was significantly smaller for square diagonal-packed square fillers than for square edge-packed fillers. The higher the constraint imposed by the filler on the deformation of the matrix, the larger the strain hardening rate. Another interesting effect was obtained when comparing circular and square fillers at same filler volume fraction and same periodic arrangement. It was concluded (Brockenbrough et al., 1991) that random distribution of squares leads to larger strain hardening rates than random distributions of circular inclusions. This was attributed to the large constraining effect of fillers with stress concentrators (sharp corners). We expect that such stress concentrations exists in our models too; however, this has no bearing on our conclusions since all composites compared here have the same filler geometry.

It may be observed that the effect described here can be interpreted to some extent as a size effect. As discussed in Section 2, no scale decoupling exists in the fractal case. For given model size, L, the truncation of the hierarchy is more pronounced as D increases since the decay of the correlation function is slower. Hence, a stronger "size effect" is expected. For imposed displacement boundary conditions, one obtains an overestimate of the elastic moduli (Huet,

1990) and, as D increases at given filler volume fraction one expects to obtain systematically larger values of the moduli. However, this is not the only reason for the larger E_e/E_1 and E_p/E_1 obtained at larger D. The stronger interaction of fillers in fractals with larger fractal dimension is responsible to a larger extent for the effect discussed in this section.

3.2. Internal stresses

The stress distribution in the microstructure is also of interest. The maximum principal stress controls fracture under monotonic and fatigue loading conditions. Probability distribution functions (PDF) of the stress in the matrix elements have been computed for all microstructures. Fig. 6(a) shows the distribution function of the maximum (tensile) principal stress in the fractal microstructure with $M = 9$, $P = 6$ and $n = 5$, along with the PDF of the same quantity in the matrix of the material with random microstructure of same volume fraction ($f = 0.131$). The far field loading is uniaxial tension and the stress is evaluated at a total strain of 2%. The stress was normalized in both cases by the far field mean stress: $0.012E_1$ for the random microstructure, and $0.0122E_1$ for the fractal microstructure. Therefore, the means of the two normalized PDFs are at 1. It is seen that the distribution corresponding to the fractal microstructure is shifted to smaller values of stress. However, the decay of the tails is much slower. The tails at large stresses cross over, with the fractal carrying more extreme stress values than the random microstructure. This discussion holds for other fractal cases as well.

It is also interesting to look at the PDF of the pressure within inclusions. As discussed in the introduction, this is relevant for situations in which fillers are used to toughen a brittle polymer. Toughening of epoxies using rubbery particles (e.g. Hayes and Seferis, 2001; Kinloch, 2003) is currently used in commercial products. In these applications, the hydrostatic stress in inclusions produces cavitation and/or filler–matrix interface debonding. Energy dissipation, leading to macroscopic toughness, is due to both the deformation of inclusions during the cavitation process, and the plastic deformation of the matrix between inclusions. The matrix plastic deformation is promoted by the release of the triaxial stress state as a consequence of filler cavitation. Recently it was suggested that the dominant effect is the dissipation in the matrix.

Fig. 6(b) shows the PDF of the hydrostatic stress ($\sigma_h = \sigma_{ii}/3$) in inclusions for the fractal case with $M = 9$, $P = 6$ and $n = 5$, and for the random microstructure of same volume fraction. The horizontal axis is normalized such to bring the two PDFs to mean 1. A more significant difference is observed in this case, with the fractal microstructure having a broader PDF, and exhibiting a slowly decaying tail on the tensile side of the distribution. This indicates that in fractal microstructures cavitation occurs at a lower far field stress. Considering that fractal microstructures are in average stiffer than their random counterparts, the observation suggests that cavitation occurs at smaller strains, which is beneficial in most applications. The origin of the different PDF of the fractal microstructure can be associated with the stronger interaction of inclusions in this type of geometry. The inter-particle distance has a broader distribution function than in the random microstructure case and hence inclusion interactions and the plastic deformation of matrix ligaments between inclusions are more pronounced.

3.3. Damping behavior

The damping behavior of these composites is discussed next. This is relevant for many applications in which composites are used as energy absorbing materials. In such situations, it is useful to inquire how should the inclusions be distributed in order to obtain maximum damping at given volume fraction of filler material. The objective of this section is to provide a quantitative assessment of this issue and to determine the role of the spatial correlation of the distribution of inclusions in defining the damping behavior of the composite.

Two situations are discussed. In the first case the matrix is considered linear elastic with no damping and dissipation being allowed within inclusions. In the second case, both matrix and inclusions are linear elastic and non-dissipative, while damping is introduced in the interfaces. These two limit situations are representative for different classes of composites and the results are expected to shed

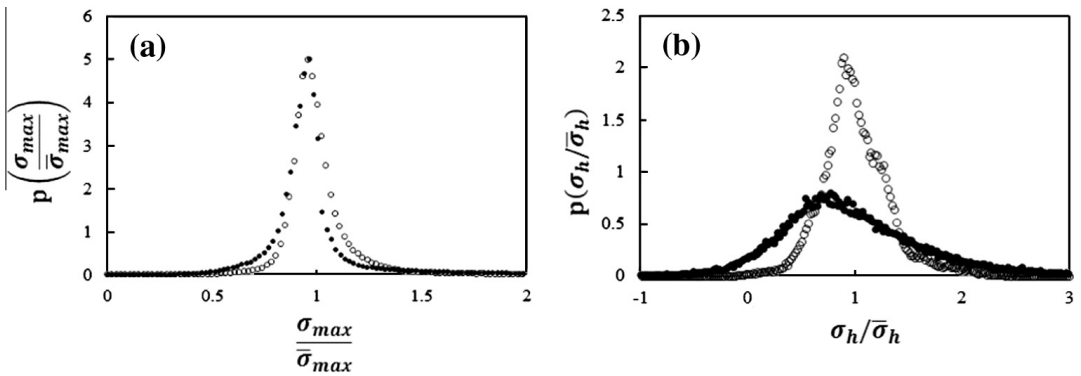

Fig. 6. Probability distribution functions for (a) the maximum principal stress in the matrix, σ_{max}, and (b) the hydrostatic stress in inclusions, σ_h, in a fractal microstructure with $M = 9$, $P = 6$, $n = 5$ (filled symbols) and the random microstructure with the same filler volume fraction (open symbols). These quantities are normalized with the respective far-field (or system average) values.

light on the microstructural optimization of these materials.

Structures similar with those in Fig. 1 are modeled using finite elements. The equation of motion is of the form:

$$[M]\{\ddot{u}\} + [C]\{\dot{u}\} + [K]\{u\} = \{0\}, \tag{7}$$

where $[M]$, $[C]$ and $[K]$ are the mass, viscous damping and stiffness matrices. A solution of the form $\{u\} = \{\phi\}e^{\lambda t}$ is sought for Eq. (7), which leads to an eigenvalue problem with eigenvalues appearing in complex conjugate pairs of the form $\lambda_r = \sigma_r \pm i\omega_r$, $r = 1,\ldots,n$, where n is the total number of degrees of freedom of the problem. For subcritical damping, the damping ratio

$$\zeta_r = -\frac{\sigma_r}{\sqrt{\sigma_r^2 + \omega_r^2}} \tag{8}$$

defines the ratio between the damping coefficient and the critical damping coefficient for mode r. Note that for proportional damping, the relation $\omega_{0r} = \sqrt{\omega_r^2 + \sigma_r^2}$ can be written between the eigenfrequency of mode r with damping, ω_r, and the corresponding eigenfrequency of the undamped system, ω_{0r}. Therefore, ω_{0r} is always larger than ω_r. Below, we report the damping ratio ζ_1 corresponding to the mode with lowest eigenfrequency.

When energy dissipation takes place only in interfaces between fillers and matrix, interface elements are used to introduce damping.

3.3.1. Damping in the filler volume

Fig. 7 shows the damping ratio for the lowest eigenfrequency mode, ζ_1, function of the volume fraction of inclusions for various systems. The open symbols and the thick line correspond to the random distribution of inclusions (Fig. 1(b)), while the other symbols correspond to fractal microstructures with various fractal dimensions. As in

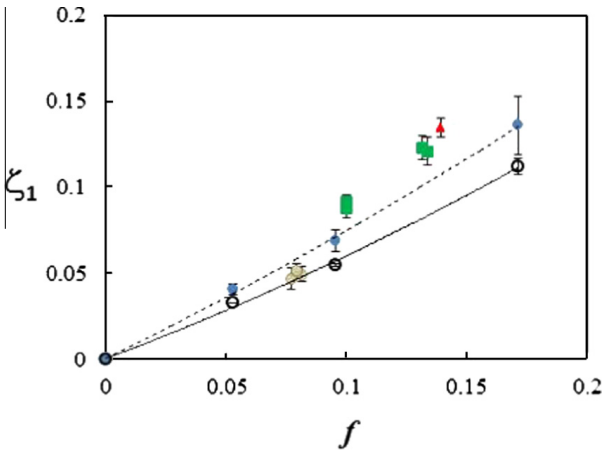

Fig. 7. Variation of the damping ratio, Eq. (8), with the volume fraction for composites with random (open circles) and fractal microstructures. The continuous and dashed lines are fitted to the results for random and fractal ($M = 9$, $P = 5$, blue circles) microstructures. The other filled symbols correspond to fractal microstructures with $M = 4$, $P = 3$, $n = 7$ and 8, $M = 9$, $P = 6$, $n = 4$ and 5 (green squares), $M = 81$, $P = 42$, $n = 2$ (red triangles), $M = 36$, $P = 10$, $n = 2$, $M = 49$, $P = 14$, $n = 2$, $M = 64$, $P = 18$, $n = 2$ (gray circles). (For interpretation of the references to color in this figure legend, the reader is referred to the web version of this article.)

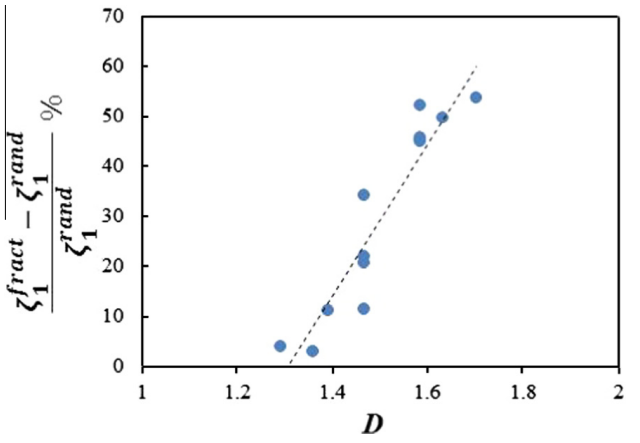

Fig. 8. Increase of the damping ratio in fractal microstructures relative to the corresponding random microstructures of same volume fraction, versus the fractal dimension, D.

Fig. 4, the dashed line is fitted to the blue circles which correspond to fractal structures with $M = 9$, $P = 5$ and various n values. The data points and error bars are evaluated from sets of 100 replicas for each configuration.

As the fractal dimension increases, the departure from the random case is more pronounced. For the fractal structure with the largest fractal dimension considered, $M = 91$, $P = 42$, $n = 3$, $D = 1.701$, the damping ratio is 53% larger than that for the random microstructure of same volume fraction. This significant increase is due entirely to the interaction between inclusions which is enhanced by their hierarchical distribution.

All fractal structures considered exhibit enhancements relative to the corresponding random cases, the increase being function of D. Fig. 8 shows the percentage increase of the damping ratio relative to the random case of same volume fraction versus the fractal dimension, for all cases considered. A linear relationship emerges, with gains close to 100% for fractal dimensions close to 1.9.

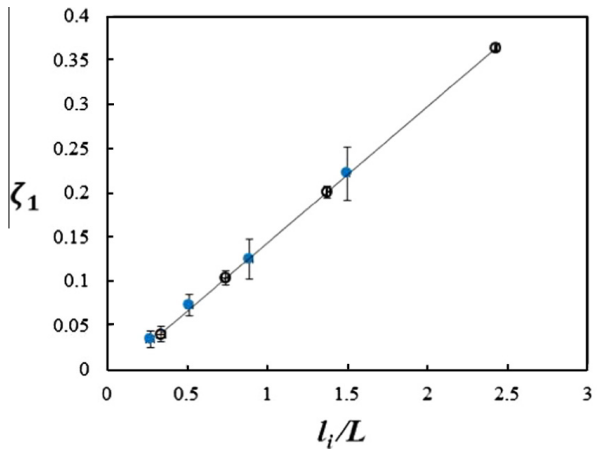

Fig. 9. Variation of the damping ratio with the total length of interfaces per unit area of the model, for the case in which damping takes place in the interfaces between matrix and fillers only, for random microstructures (open symbols and line) and for fractal microstructures with $M = 9$, $P = 5$ and $n = 2$–5 (blue filled symbols). (For interpretation of the references to color in this figure legend, the reader is referred to the web version of this article.)

3.3.2. Damping in the filler–matrix interfaces

Let us consider now that both matrix and filler materials are linear elastic and non-dissipative, and dissipation takes place in the interface between matrix and inclusions. The comparison is performed between composites with fractal and random microstructures having the same total interface length.

Fig. 9 shows the damping ratio corresponding to the lowest eigenfrequency mode for fractal microstructures with $M = 9$, $P = 5$ and $n = 2$–5, and for the corresponding random microstructures. The emerging physical picture is quite different from that discussed in Section 3.3.1. The damping ratio increases linearly with the total interfacial length, and the way the inclusions are distributed has no influence on the overall dissipation. This observation is interesting and provides guidance to composite design for damping applications.

4. Conclusions

The objective of this work is to establish the role of spatial correlations of the distribution of inclusions in defining the mechanical behavior of particulate composites. In particular, fractal microstructures having power law-correlated characteristic functions are compared with random microstructures which have no spatial correlation. The central question is whether fractal microstructures have enhanced properties relative to the random microstructures with identical filler volume fraction.

It is observed that composites with fractal microstructures are stiffer and have larger strain hardening rates, the effect increasing with the fractal dimension. A pronounced effect results when both materials are elastic, but energy dissipation is allowed within fillers. In this case, fractal microstructures dissipate up to 100% more energy compared with the random microstructures of same filler volume fraction. Interestingly, if viscous damping is introduced only in the interface between fillers and matrix, the distribution of inclusions has no effect on the overall damping of the composite.

On the local scale, the pressure within inclusions has more extreme values in the fractal composite. This is important in situations in which cavitation in inclusions is used as a method to enhance the toughness of the composite. The present results indicate that cavitation takes place at a lower overall stress in the composite with fractal microstructure.

In conclusion, microstructures with long-range correlated distributions of inclusions are preferable in some applications, as they exhibit significantly different behavior relative to that of composites with random distribution of inclusions. However, the mechanical response of fractal microstructures depends on the range of scales of the fractal hierarchy and indirectly on the model/sample size relative to the size of the smallest inclusions. This size effect is absent in the case of random microstructures or microstructures with short-range correlations, provided the model is at least an order of magnitude larger than the correlation length.

The present results can be used to improve the design of composites for structural applications. At present, the only technology able to produce microstructures with specific distributions of inclusions is additive manufacturing. The low throughput and rather large cost of these methods prohibit their use for large scale composite fabrication, except in few cases, such as when the final product is in the form of thin films. Powder metallurgy and electrolytic co-deposition have been used to fabricate composites with graded compositions, however, these methods do not insure obtaining the desired, position independent spatial correlation of properties discussed here. Further research is needed in the manufacturing area to develop methods adequate for the fabrication of such materials.

Acknowledgments

This work was supported in part by a grant from the Romanian National Authority for Scientific Research, CNCS – UEFISCDI, project number PN-II-ID-PCE-2011-3-0120, contract 293/2011.

References

Argyris, J., Ciubotariu, C.I., Weingaertner, W.E., 2000. Fractal space signatures in quantum physics and cosmology – I. Space, time, matter, fields and gravitation. Chaos Solitons Fractals 11, 1671–1719.

Bako, B., Hoffelner, W., 2007. Cellular dislocations patterning during plastic deformation. Phys. Rev. B 76, 214108.

Banissadi, M., Ahzi, S., Garmestani, H., Ruch, D., Remond, Y., 2012. New approximate solution for *N*-point correlation functions for heterogeneous materials. J. Mech. Phys. Solids 60, 104–119.

Baxter, R.J., 1982. Exactly Solved Models in Statistical Mechanics. Academic Press, London.

Bazant, Z., 1997. Scaling of quasibrittle fracture: hypotheses of invasive and lacunar fractality, their critique and Weibull connection. Int. J. Frac. 83, 41–65.

Beran, M.J., Molyeux, J., 1966. Continuum Theories. Wiley, NY.

Bergman, D.J., Kantor, Y., 1984. Critical properties of an elastic fractal. Phys. Rev. Lett. 53, 511–514.

Brockenbrough, J.R., Suresh, S., Wienecke, H.A., 1991. Acta Metall. Mater. 39, 735.

Carpinteri, A., Chiaia, B., Cornetti, P., 2004. A fractal theory for the mechanics of elastic materials. Mater. Sci. Eng. A 365, 235–240.

Chen, Y.S., Choi, W., Papanikolaou, S., Sethna, J.P., 2010. Bending crystals: emergence of fractal dislocation structures. Phys. Rev. Lett. 105, 105501.

Dvorak, G.J., 2013. Mechanics of Composite Materials. Springer, New York.

Dyskin, A.V., 2005. Effective characteristics and stress concentrations in materials with self-similar microstructure. Int. J. Solids Struct. 42, 477–502.

Dzhaparidze, K., van Zanten, H., 2003. Krein's spectral theory and the Paley–Wiener expansion for fractional brownian motion. Stochastic Section Report 13. Vrije Univ., Amsterdam.

Falconer, K., 2003. Fractal Geometry – Mathematical Foundations and Applications. Wiley, Sussex. England.

Ghanem, R., Dham, S., 1998. Stochastic finite element analysis for multiphase flow in heterogeneous porous media. Transport Porous Med. 32, 239–262.

Ghanem, G., Spanos, P.D., 1991. Stochastic Finite Elements: A Spectral Approach. Springer-Verlag, New York.

Gneiting, T., Schlather, M., 2004. Stochastic models that separate fractal dimension and Hurst effect. SIAM Rev. 46, 269–282.

Hashin, Z., 1965. On elastic behavior of fiber reinforced materials of arbitrary transverse phase geometry. J. Mech. Phys. Solids 13, 119–134.

Hashin, Z., Shtrikman, S., 1962. On some variational principles in anisotropic and nonhomogeneous elasticity. J. Mech. Phys. Solids 10, 335–342.

Hayes, B.S., Seferis, J.C., 2001. Modification of thermosetting resins and composites through preformed polymer particles: a review. Polym. Compos. 22, 451–467.

Huet, C., 1990. Application of variational concepts to size effects in elastic heterogeneous bodies. J. Mech. Phys. Solids 38, 813–841.
Kinloch, A.J., 2003. Toughening epoxy adhesives to meet today's challenges. MRS Bull. 28, 445–448.
Kolwankar, K.M., 1998. Studies of Fractal Structures and Processes Using Methods of Fractional Calculus (Ph.D. thesis). University of Pune, India.
Kolwankar, K.M., Gangal, A.D., 1996. Fractional differentiability of nowhere differentiable functions and dimensions. Chaos 6, 505–524.
Liu, W.K., Belytschko, T., Mani, A., 1986. Probabilistic finite elements for nonlinear structural dynamics. Comput. Meth. Appl. Mech. Eng. 56, 61–81.
Liu, W.K., Mani, A., Belytschko, T., 1987. Finite element methods in probabilistic mechanics. Prob. Eng. Mech. 2, 201–213.
Mandelbrot, B.B., 1983. The Fractal Geometry of Nature. Freeman, New York.
Matthies, H.G., Brenner, C.E., Bucher, C.G., Soares, C.G., 1997. Uncertainties in probabilistic numerical analysis of structures and solids – stochastic finite elements. Struct. Saf. 19, 283–336.
Meyers, M.A., Lin, A.Y.M., Seki, Y., Chen, P.Y., Kad, B.K., Bodde, S., 2006. Structural biological composites: an overview. J. Mater. 58, 35–41.
Milton, G.W., 1981. Bounds on the electromagnetic, elastic, and other properties of two-component composites. Phys. Rev. Lett. 46, 542–545.
Milton, G.W., 1982. Bound on the elastic and transport properties of two component composites. J. Mech. Phys. Sol. 30 (3), 177–191.
Nakamura, T., Suresh, S., 1993. Effect of thermal residual stress and fiber packing on deformation of metal–matrix composites. Acta Metall. Mater. 41, 1665–1681.
Nemat-Nasser, S., Hori, M., 1999. Micromechanics: Overall Properties of Heterogeneous Materials. North-Holland, Amsterdam.
Oshmyan, V.G., Patlashan, S.A., Timan, S.A., 2001. Elastic properties of Sierpinski-like carpets: finite-element-based simulation. Phys. Rev. E 64, 1–10, 056108.
Ostoja-Starzewski, M., 2007. Towards thermoelasticity of fractal media. J. Therm. Stresses 30, 889–896.
Ostoja-Starzewski, M., 2009. Extremum and variational principles for elastic and inelastic media with fractal geometries. Acta Mech. 205, 161–170.
Ostoja-Starzewski, M., 2012. Elastic-plastic transitions in 3D random materials: massively parallel simulations, fractal morphogenesis and scaling functions. Philos. Mag. 92, 2733–2758.
Papadrakakis, M., Papadopoulos, V., 1996. Robust and efficient methods for stochastic finite element analysis using Monte Carlo simulations. Comput. Meth. Appl. Mech. Eng. 134, 325–340.
Parkinson, I.H., Fazzalari, N.L., 2000. Methodological principles for fractal analysis of trabecular bone. J. Microsc. 198, 134–142.
Phan-Tien, N., Milton, G.W., 1982. New bounds on the effective thermal conductivity of *n*-phase materials. Proc. R. Soc. London A 380, 333–348.
Picu, R.C., Soare, M.A, 2009. Mechanics of materials with self-similar hierarchical microstructure. In: Galvanetto, U., Aliabadi, M.F. (Eds.), Multiscale Modeling in Solid Mechanics – Computational Approaches. Imperial College Press, London, pp. 295–332.
Quinatanilla, J., Torquato, S., 1995. New bounds on the elastic moduli of suspensions of spheres. Appl. Phys. 77, 4361–4372.
Salganik, R.L., 1973. Mechanics of bodies with many cracks. Mech. Solids 8, 135–143.
Silnutzer, N.R., 1972. Effective Constants of Statistically Homogeneous Materials (Ph.D. thesis). University of Pennsylvania, Philadelphia.
Soare, M.A., Picu, R.C., 2007. An approach to solving mechanics problems for materials with multiscale self-similar microstructure. Int. J. Solids Struct. 44, 7877–7890.
Soare, M.A., Picu, R.C., 2008a. Boundary value problems defined on stochastic self-similar multiscale geometries. Int. J. Numer. Methods Eng. 74, 668–696.
Soare, M.A., Picu, R.C., 2008b. Spectral decomposition of random fields defined over the generalized Cantor set. Chaos Soliton Fractals 37, 566–573.
Suresh, S., Brockenbrough, J.R., 1993. Continuum models of deformation: metals reinforced with continuous fibers. In: Suresh, S., Mortensen, A., Needleman, A. (Eds.), Fundamentals of Metal Matrix Composites. Butterworth-Heinemann.
Tarasov, V.E., 2005a. Fractional hydrodynamics equations for fractal media. Ann. Phys. 318, 286–307.
Tarasov, V.E., 2005b. Continuous medium model for fractal media. Phys. Lett. A 336, 167–174.
Torquato, S., 2002. Random Heterogeneous Materials: Microstructure and Macroscopic Properties. Springer, New-York.
Vaezi, M., Seitz, H., Yang, S., 2012. A review on 3D micro-additive manufacturing technologies. Int. J. Adv. Manuf. Tech. http://dx.doi.org/10.1007/s 00170-012-4605-2.
Witten, T.A., Sander, L.M., 1983. Diffusion-limited aggregation. Phys. Rev. 27, 5686–5697.
Zaiser, M., Hahner, P., 1999. Fractal analysis of deformation induced dislocation patterns. Acta Mater. 47, 2463–2476.